An Introduction to Isogeometric Collocation Methods

Alessandro Reali[1,2*] and Thomas J.R. Hughes[3†]

[1] Department of Civil Engineering and Architecture, University of Pavia, Italy
[2] CNR Institute of Applied Mathematics and Information Technology "E. Magenes", Pavia, Italy
[3] Institute for Computational Engineering and Sciences, University of Texas at Austin, USA.

Abstract Within the framework of isogeometric analysis, collocation methods have been recently proposed as an interesting strong form alternative to standard Galerkin approaches, characterized by a significantly reduced computational cost, but still guaranteeing higher order convergence rates. In this chapter we provide a concise introduction to isogeometric collocation methods and propose a brief review of some of the most important results obtained so far in this context.

1 Introduction

The main aim of Isogeometric analysis (IGA), introduced ten years ago by Hughes et al. (2005), is to bridge the gap between Computer Aided Design (CAD) and Finite Element Analysis (FEA). Accordingly, the basic IGA paradigm consists of adopting the same basis functions used for geometry representations in CAD systems - such as, e.g., Non-Uniform Rational B-Splines (NURBS) - for the approximation of field variables, in an isoparametric fashion. This leads to a cost-saving simplification of the typically expensive mesh generation and refinement processes required by standard FEA. Moreover, thanks to the high-regularity properties of its basis functions, IGA has shown a better accuracy per-degree-of-freedom and an enhanced robustness with respect to standard FEA in a number of

*A. Reali was supported by the European Research Council (ERC grant "ISOBIO", agreement no. 259229).

†T.J.R. Hughes was supported by grants from the Office of Naval Research (N00014-08-1-0992), the National Science Foundation (CMMI-01101007), and SINTEF (UTA10-000374) with the University of Texas at Austin.

applications ranging from solids and structures (see, e.g., Auricchio et al., 2010b; Borden et al., 2012; Caseiro et al., 2014; Cottrell et al., 2006, 2007; de Falco et al., 2011; Dhote et al., 2014; Elguedj et al., 2008; Hughes et al., 2008, 2014; Lipton et al., 2010; Morganti et al., 2014; Reali, 2006) to fluids (see, e.g., Akkerman et al., 2007; Bazilevs et al., 2007; Bazilevs and Hughes, 2008; Buffa et al., 2011; Liu et al., 2014; Gomez et al., 2010), opening also the door to geometrically flexible discretizations of higher-order partial differential equations in primal form (see, e.g., Auricchio et al., 2007; Gomez et al., 2008; Kiendl et al., 2009).

It is well known that an important issue related to IGA concerns the development of efficient integration rules, able to reduce assembly costs in particular when higher-order approximations are employed. The fact that element-wise Gauss quadrature, typically used for standard FEA and originally adopted for Galerkin-based IGA, does not properly take into account the inter-element higher continuity of the IGA basis functions leads to suboptimal assembly costs, significantly affecting the performance of IGA methods. Ad hoc quadrature rules have been proposed by Hughes et al. (2010), Auricchio et al. (2012b), and Schillinger et al. (2014a), but the development of a general and effective solution for Galerkin-based IGA methods is still an open problem.

Aiming at optimizing the computational cost, still taking advantage of IGA geometrical flexibility and accuracy, isogeometric collocation schemes have been recently proposed by Auricchio et al. (2010a, 2012a). The fundamental idea consists of the discretization of the governing partial differential equations in strong form, adopting the isoparametric paradigm and making use of the higher-continuity properties of the IGA shape functions. Detailed comparisons with both IGA and FEA Galerkin-based approaches have shown IGA collocation advantages in terms of accuracy versus computational cost, in particular when higher-order approximation degrees are adopted (Schillinger et al., 2013). In general, IGA collocation features look particularly desirable in all those situations where evaluation and assembly costs are dominant, as in the case of explicit structural dynamics where the computational cost is dominated by stress divergence evaluations at quadrature points for the calculation of the residual force vector (Auricchio et al., 2012a; Schillinger et al., 2013).

Within the IGA collocation context, several promising significant studies have been recently published, including phase-field modeling (Gomez et al., 2014), contact (De Lorenzis et al., 2014b), and hierarchical local refinement (Schillinger et al., 2013). Moreover, IGA collocation has been very successful in the context of structural elements. In particular, Bernoulli-Euler beam and Kirchhoff plate elements have been proposed by Reali and Gomez

(2014), and shear-deformable structural elements have been considered in a number of papers. Mixed formulations both for Timoshenko initially-straight planar beams (Beirão da Veiga et al., 2012) and for curved spatial rods (Auricchio et al., 2013) have been proposed and studied. Isogeometric collocation has been moreover successfully applied to the solution of Reissner-Mindlin plate problems in Kiendl et al. (2014a). Finally, a new single-parameter formulation for shear-deformable beams, recently introduced by Kiendl et al. (2014b), has been solved also via IGA collocation.

It is therefore clear that, thanks to its interesting and promising features, IGA collocation has attracted and is increasingly attracting a good deal of interest among Computational Mechanics researchers. This chapter is aimed to people who desire to get acquainted with the basic concepts of IGA collocation, and its goal is to provide a concise introduction, as well as to propose a brief review of some of the most important results obtained so far in this context.

2 Basics of NURBS-Based IGA Collocation

In this section, we aim at introducing the basic concepts of NURBS-based IGA collocation. After some preliminaries on B-Splines and NURBS, we introduce the idea of collocation in a very simple 1D setting, presenting also some theoretical and numerical results.

2.1 B-Spline and NURBS preliminaries

In the following, we briefly introduce the basic definitions and notations about B-Splines and NURBS. For further details, readers are referred to Piegl and Tiller (1997), Cottrell et al. (2009), and references therein.

A B-Spline basis function of degree p is generated starting from a non-decreasing sequence of real numbers referred to as knot vector

$$\Xi = \{\xi_1, ..., \xi_{m+p+1}\} \tag{1}$$

where m is the number of basis functions (equal to the number of the associated control points). A univariate B-Spline basis function $N_{i,p}(\xi)$ can be then constructed using the following Cox-de Boor recursion formula: Starting from $p = 0$, where

$$N_{i,0}(\xi) = \begin{cases} 1 & \xi_i \leq \xi < \xi_{i+1} \\ 0 & \text{otherwise} \end{cases} \tag{2}$$

the basis functions for $p > 0$ are obtained from

$$N_{i,p}(\xi) = \frac{\xi - \xi_i}{\xi_{i+p} - \xi_i} N_{i,p-1}(\xi) + \frac{\xi_{i+p+1} - \xi}{\xi_{i+p+1} - \xi_{i+1}} N_{i+1,p-1}(\xi) \tag{3}$$

where the convention $0/0 = 0$ is assumed. Given the multiplicity k of a knot, the smoothness of the B-Spline basis is C^{p-k} at that location, while it is C^{∞} everywhere else. In so-called open knot vectors, the first and the last knots have multiplicity $k = p + 1$ and the basis is interpolatory at the ends (see, e.g., Figure 1).

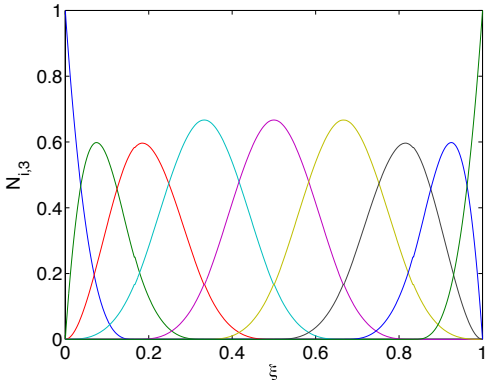

Figure 1. Cubic B-Spline basis functions formed from the open knot vector $\Xi = \{0, 0, 0, 0, 1/6, 1/3, 1/2, 2/3, 5/6, 1, 1, 1, 1\}$.

A B-Spline curve can be then constructed as the linear combination of the basis functions

$$\mathbf{C}(\xi) = \sum_{i=1}^{m} N_{i,p} \mathbf{P}_i \tag{4}$$

where the coefficients $\mathbf{P}_i \in \mathbb{R}^{d_s}$ of the linear combination are the so-called control points, being d_s the dimension of the physical space (see, e.g., Figure 2).

Multivariate B-Splines are generated through the tensor product of univariate B-Splines. If d_p denotes the dimension of the parametric space, d_p univariate knot vectors are needed:

$$\Xi^d = \left\{ \xi_1^d, ..., \xi_{m_d + p_d + 1}^d \right\} \tag{5}$$

where $d = 1, ..., d_p$, p_d is the polynomial degree in the parametric direction d, and m_d is the associated number of basis functions. Denoting the univariate

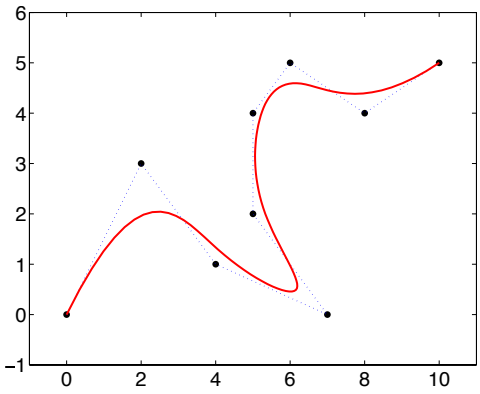

Figure 2. A 2D piecewise cubic B-Spline curve generated from the basis functions of Figure 1 (solid line), along with its control points (black dots), and control net (dotted line)

basis functions in each parametric direction ξ^d by $N^d_{i_d,p_d}$, the multivariate basis functions $B_{\mathbf{i},\mathbf{p}}(\boldsymbol{\xi})$ are obtained as

$$B_{\mathbf{i},\mathbf{p}}(\boldsymbol{\xi}) = \prod_{d=1}^{d_p} N^d_{i_d,p_d}\left(\xi^d\right) \tag{6}$$

where the multi-index $\mathbf{i} = \left\{i_1, ..., i_{d_p}\right\}$ denotes the position in the tensor product structure, $\mathbf{p} = \{p_1, ..., p_d\}$ indicates the polynomial degrees, and $\boldsymbol{\xi} = \left\{\xi^1, ..., \xi^{d_p}\right\}$ is the vector of the parametric coordinates in each parametric direction d. B-Spline surfaces and solids are obtained, for $d_p = 2$ and $d_p = 3$, respectively, from a linear combination of multivariate B-Spline basis functions and control points as follows

$$\mathbf{S}(\boldsymbol{\xi}) = \sum_{\mathbf{i}} B_{\mathbf{i},\mathbf{p}}(\boldsymbol{\xi})\,\mathbf{P}_{\mathbf{i}} \tag{7}$$

where the summation is extended to all combinations of the multi-index $\mathbf{i}$.

NURBS basis functions in $\mathbb{R}^{d_s}$ are obtained from a projective transformation of their B-Spline counterparts in $\mathbb{R}^{d_s+1}$. Univariate NURBS basis functions $R_{i,p}(\xi)$ are given by

$$R_{i,p}(\xi) = \frac{N_{i,p}(\xi)\,w_i}{\sum_{j=1}^{m} N_{j,p}(\xi)\,w_j} \tag{8}$$

where $N_{i,p}$ are B-Spline basis functions and w_i are the corresponding weights (i.e., the (d_s+1)-th coordinates of the B-Spline control points in $\mathbb{R}^{d_s+1}$). Finally, multivariate NURBS basis functions are obtained as

$$R_{\mathbf{i},\mathbf{p}}(\boldsymbol{\xi}) = \frac{B_{\mathbf{i},\mathbf{p}}(\boldsymbol{\xi})\, w_{\mathbf{i}}}{\sum_{\mathbf{j}} B_{\mathbf{j},\mathbf{p}}(\boldsymbol{\xi})\, w_{\mathbf{j}}} \tag{9}$$

and NURBS surfaces and solids are constructed as

$$\mathbf{S}(\boldsymbol{\xi}) = \sum_{\mathbf{i}} R_{\mathbf{i},\mathbf{p}}(\boldsymbol{\xi})\, \mathbf{P}_{\mathbf{i}} \tag{10}$$

2.2 IGA collocation in 1D

In this section, we introduce the basic ideas of IGA collocation in a very simple 1D setting. We also discuss the choice of collocation points and propose some theoretical results. We then conclude the section presenting some numerical tests.

Formulation. Let f, a_0, a_1, be real functions in $C^0[a,b]$, with $a<b$ given real numbers. Let $g_0, g_1 \in \mathbb{R}$ be scalars and $\mathcal{B}C_0, \mathcal{B}C_1 : C^1[a,b] \to \mathbb{R}$ be linear operators. We are interested in the following simple one-dimensional model differential problem. Find a real function $u \in C^2[a,b]$ such that

$$\begin{cases} u''(x) + a_1(x)u'(x) + a_0(x)u(x) = f(x) & \forall x \in (a,b) \\ \mathcal{B}C_i(u) = g_i & i = 0,1 \end{cases} \tag{11}$$

where u', u'' represent the first and second derivatives of u, respectively (we note that in the following we will indicate the derivative operator of order i also as D^i, $i \in \mathbb{N}$). We assume that (11) has one and only one solution u, and that the boundary condition operators $\mathcal{B}C_i$ are linearly independent on $\mathrm{Ker}(D^2)$, that is, on the space of linear functions.

To discretize problem (11) via IGA collocation, we proceed as follows. Given $n \in \mathbb{N}$, let $\mathcal{V}_{n+2} \subset C^2[a,b]$ be a NURBS space of dimension $n+2$ on the interval $[a,b]$, associated with a spline space $\hat{\mathcal{S}}_{n+2} \subset C^2[0,1]$ on the parametric interval $[0,1]$. With standard assumptions on the one-dimensional geometrical map F, we consider $DF > 0$ on the parametric domain $[0,1]$. Given, for all $n \in \mathbb{N}$, $\tau_1 < \tau_2 < ... < \tau_n$ assigned collocation points in $[a,b]$, we obtain the following discrete problem: Find $u_n \in \mathcal{V}_{n+2}$ such that

$$\begin{cases} u_n''(\tau_j) + a_1(\tau_j)u_n'(\tau_j) + a_0(\tau_j)u_n(\tau_j) = f(\tau_j) & j = 1,..,n \\ \mathcal{B}C_i u_n = g_i \qquad i = 0,1 \end{cases} \tag{12}$$

It is to be remarked that this formulation gives rise in general to a non-symmetric (but diagonally dominant) system matrix.

Collocation points and theoretical results. The discrete problem (12) is defined once a strategy for the selection of the n collocation points is set. Such a selection is of paramount importance, because it directly influences the stability and convergence properties of the collocation scheme.

In the IGA collocation literature, the images of so-called Greville abscissae (see de Boor, 2001) have been widely adopted as the default choice for collocation points. Greville abscissae are n points easily defined from the knot vector as

$$\overline{\xi}_i = (\xi_{i+1} + \xi_{i+2} + ... + \xi_{i+p})/p \tag{13}$$

and are well known in the CAD literature for a number of properties, among which the fact that they typically give a stable interpolation (except in some cases when high degrees are combined with particular non-uniform meshes[1]).

The selection of points guaranteeing a stable interpolation is a fundamental issue for a collocation scheme, since it is proven in Auricchio et al. (2010a) that this implies optimal convergence (i.e., of order $p-1$) in the $W^{2,\infty}$-norm (or, equivalently, in the H^2-norm).

Unfortunately, such a proof is valid only in 1D and cannot be extended to higher dimensions. However, as we will also see in the following sections, extensive numerical testing has shown that the convergence rates obtained in 1D are attained also in higher dimensions.

Moreover, optimal convergence rates are not recovered in the L^∞- and $W^{1,\infty}$-norms (or, equivalently, in the L^2- and H^1-norms), where it has been numerically shown (see, e.g., next section) that orders of convergence p and $p-1$ for even and odd degrees, respectively, are attained.

It is important to note that, despite not being optimal in the L^2- and H^1-norms (except in the case of the H^1-norm for p even) as it happens instead for Galerkin methods, the obtained orders of convergence are increasing with p, whereas the cost of collocation is much lower than that of Galerkin approaches of the same order, especially as p increases. This makes IGA collocation very competitive with respect to Galerkin on the basis of an accuracy-to-computational-cost ratio, in particular when higher degrees (e.g., $p > 3$) are adopted. More details in this sense will be given later in the framework of 3D elasticity, and interested readers are referred to the comprehensive study reported in Schillinger et al. (2013).

[1] An alternative that is proven to be always stable is given by the so-called Demko abscissae (Demko, 1985), which can be computed by an iterative algorithm (see Auricchio et al., 2010a, for more details and for a discussion on their use within IGA collocation).

Numerical results. We now present some numerical experiments in 1D confirming the convergence rates previously discussed.

In particular, we consider the following model problem defined on the domain $[0, 1]$:

$$\begin{cases} -u'' + u' + u = (1 + 4\pi^2)\sin(2\pi x) - 2\pi\cos(2\pi x), & \forall x \in (0, 1) \\ u(0) = u(1) = 0 \end{cases} \tag{14}$$

which admits the exact solution:

$$u = \sin(2\pi x) \tag{15}$$

This problem is numerically solved using the collocation method outlined in the previous sections, adopting Greville abscissae as collocation points. In Figures 3-5, we report log-scale plots of the relative errors for different degrees of approximations in L^∞-, $W^{1,\infty}$-, and $W^{2,\infty}$-norms, respectively. The obtained results show that in the first two norms an order of convergence p is attained for even degrees, while an order $p-1$ is attained for odd degrees. Instead in the $W^{2,\infty}$-norm, we observe the expected optimal order of convergence, i.e., $p-1$, for all approximation degrees, in agreement with the predictions of the theory[2].

More results, considering the influence of a nonlinear parameterization, of different choices of collocation points like Demko abscissae, and of Neumann boundary conditions, may be found in Auricchio et al. (2010a).

Spectral approximation. One of the most important results of Galerkin IGA, with a fundamental impact on the solution of structural dynamics problems, is its capability of approximating higher modes, without introducing spurious "optical branches" in the numerical spectrum (see Cottrell et al., 2006; Reali, 2006; Hughes et al., 2008, 2014). The same capabilities are present also in IGA collocation, as it has been shown in Auricchio et al. (2010a). To this end, the following 1D eigenvalue problem is considered

$$\begin{cases} u'' + \omega^2 u = 0 & \forall x \in (0, 1) \\ u(0) = u(1) = 0 \end{cases} \tag{16}$$

[2] In Figures 3-5, we have not included results for $p = 2$, since this case is not covered by the theory of Auricchio et al. (2010a). However, the results obtained are in complete agreement with the ones observed for higher degrees, i.e., order p for the L^∞- and $W^{1,\infty}$-norms and $p-1$ for the $W^{2,\infty}$-norm (see also the numerical results of next section).

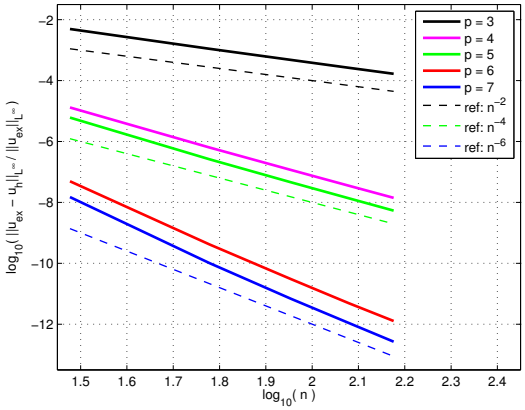

Figure 3. 1D model problem. Relative error in L^∞-norm for different degrees of approximation.

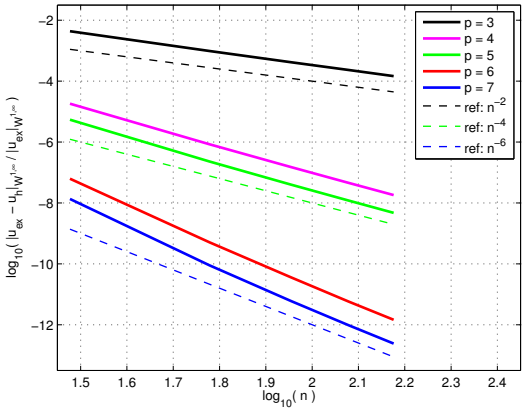

Figure 4. 1D model problem. Relative error in $W^{1,\infty}$-norm for different degrees of approximation.

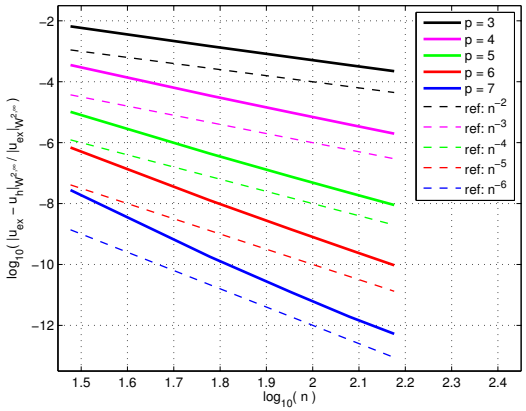

Figure 5. 1D model problem. Relative error in $W^{2,\infty}$-norm for different degrees of approximation.

for which the exact frequencies ω_n are given by

$$\omega_n = 2\pi n \qquad \text{with } n = 1, 2, 3, \dots \tag{17}$$

Problem (16) is solved using the collocation method with Greville abscissae and, in Figure 6, we report the results in terms of normalized discrete spectra, obtained considering a linear parameterization and using different degrees of approximation (1000 d.o.f.'s have been used to produce each spectrum). It is possible to observe the good behavior of all spectra, which converge for an increasing degree p as it happens with Galerkin IGA (for more details on eigenvalue problems solved via IGA collocation, see Auricchio et al., 2010a).

3 NURBS-Based IGA Collocation for Linear Elastostatics

In this section, we extend the previously introduced IGA collocation methods to the multi-dimensional case, considering in particular linear elastostatics as model problem. Accordingly, in the following, we present the basic equations of linear elastostatics and introduce an IGA collocation formulation to solve them. Several numerical tests are proposed to show the behavior of the proposed formulation, as well as to compare its perfor-

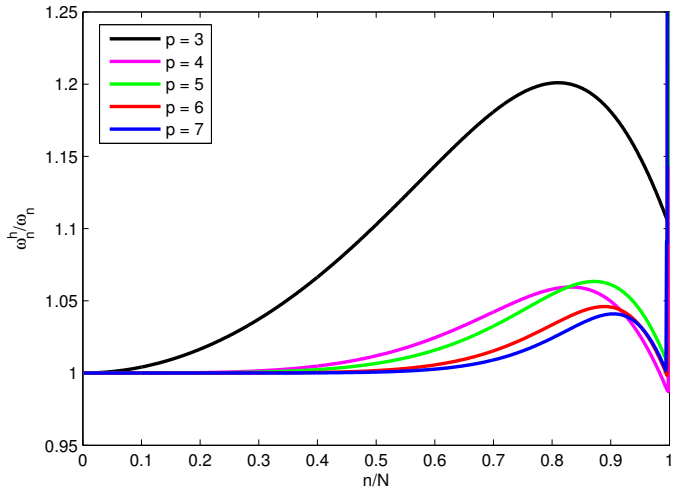

Figure 6. 1D eigenvalue problem with linear parameterization using Greville abscissae. Normalized spectra for different degrees of approximation.

mance with that of Galerkin IGA and FEA on the basis of the accuracy-to-computational-cost ratio.

3.1 Linear elastostatics

Let $\Omega \subset \mathbb{R}^{d_s}$ represent an elastic body $\mathcal{B}$ subjected to body forces $\mathbf{f}$, to prescribed displacements $\mathbf{g}$ on a portion of the boundary Γ_g, and to (possibly zero) prescribed tractions $\mathbf{p}$ on the remaining portion Γ_p, being $\Gamma = \Gamma_g \bigcup \Gamma_p$ the boundary of the domain, with $\Gamma_g \bigcap \Gamma_p = \emptyset$. Suitable regularity requirements are assumed to hold for $\mathbf{f}$, $\mathbf{g}$, and $\mathbf{p}$.

The small-strain linear elastostatics problem in strong form is defined as

$$\nabla \cdot \left(\mathbb{C}\nabla^S \mathbf{u}\right) + \mathbf{f} = \mathbf{0} \qquad \text{in } \Omega \tag{18}$$

complemented by the Dirichlet boundary conditions

$$\mathbf{u} = \mathbf{g} \qquad \text{on } \Gamma_g \tag{19}$$

and by the Neumann boundary conditions

$$\left(\mathbb{C}\nabla^S \mathbf{u}\right) \cdot \mathbf{n} = \mathbf{p} \qquad \text{on } \Gamma_p \tag{20}$$

where, $\mathbf{u}(\mathbf{x})$ is the unknown displacement field ($\mathbf{x}$ being the position vector), ∇ is the standard nabla operator and ∇^S is its symmetric part, $\mathbb{C}$ is the fourth-order elasticity tensor, and $\mathbf{n}$ is the unit outward normal to the boundary of the domain.

3.2 IGA collocation for elastostatics

As in Auricchio et al. (2012a), Schillinger et al. (2013), and De Lorenzis et al. (2014b), herein, we choose to interpret the collocation method in a variational sense and to directly apply it in the isogeometric framework. The elasticity problem in variational form, based on the principle of virtual work, reads

$$\int_\Omega \left(\mathbb{C}\nabla^S \mathbf{u}\right) : \nabla^S \mathbf{w} d\Omega = \int_\Omega \mathbf{f}\cdot\mathbf{w} d\Omega + \int_{\Gamma_p} \mathbf{p}\cdot\mathbf{w} d\Gamma \tag{21}$$

for every test function $\mathbf{w} \in \left[H^1(\Omega)\right]^{d_s}$ satisfying homogeneous Dirichlet boundary conditions, i.e.,

$$\mathbf{w} = \mathbf{0} \qquad \text{on}\, \Gamma_g \tag{22}$$

Integrating eq. (21) by parts and rearranging terms leads to

$$\int_\Omega \left[\nabla\cdot\left(\mathbb{C}\nabla^S\mathbf{u}\right) + \mathbf{f}\right]\cdot\mathbf{w} d\Omega - \int_{\Gamma_p}\left[\left(\mathbb{C}\nabla^S\mathbf{u}\right)\cdot\mathbf{n} - \mathbf{p}\right]\cdot\mathbf{w} d\Gamma = 0 \tag{23}$$

Note that, should the test function *not* satisfy eq. (22), we could release the Dirichlet boundary conditions on the solution $\mathbf{u}$ and introduce a Lagrange multiplier $\boldsymbol{\lambda} \in \left[H^{-1/2}(\Gamma_g)\right]^{d_s}$ to enforce the boundary conditions weakly. The variational form of the elasticity problem would then read: Find $(\mathbf{u}, \boldsymbol{\lambda}) \in \left[H^1(\Omega)\right]^{d_s} \times \left[H^{-1/2}(\Gamma_g)\right]^{d_s}$ such that

$$\begin{aligned}\int_\Omega \left(\mathbb{C}\nabla^S\mathbf{u}\right) : \nabla^S\mathbf{w} d\Omega = &\int_\Omega \mathbf{f}\cdot\mathbf{w} d\Omega + \int_{\Gamma_p}\mathbf{p}\cdot\mathbf{w} d\Gamma + \int_{\Gamma_g}\boldsymbol{\lambda}\cdot\mathbf{w} d\Gamma \\ &+ \int_{\Gamma_g}\boldsymbol{\mu}\cdot\left(\mathbf{u}-\mathbf{g}\right) d\Gamma\end{aligned} \tag{24}$$

for every test function pair $(\mathbf{w}, \boldsymbol{\mu}) \in \left[H^1(\Omega)\right]^{d_s} \times \left[H^{-1/2}(\Gamma_g)\right]^{d_s}$. Note that additional terms pertaining to the Dirichlet boundary have appeared above. If the solution $\mathbf{u}$ is sufficiently smooth (e.g., if $\mathbf{u} \in [H^2(\Omega)]^{d_s}$), then by elliptic regularity, it holds that $\left(\mathbb{C}\nabla^{\mathrm{S}}\mathbf{u}\right)\cdot\mathbf{n} \in \left[L^2(\Gamma_g)\right]^{d_s}$ and $\boldsymbol{\lambda} \equiv$

$\left(\mathbb{C}\nabla^{\mathrm{S}}\mathbf{u}\right)\cdot\mathbf{n}$. Consequently, if $\mathbf{u}$ is sufficiently smooth, we have

$$\int_{\Omega}\left(\mathbb{C}\nabla^{S}\mathbf{u}\right):\nabla^{S}\mathbf{w}d\Omega=\int_{\Omega}\mathbf{f}\cdot\mathbf{w}d\Omega+\int_{\Gamma_{p}}\mathbf{p}\cdot\mathbf{w}d\Gamma+\int_{\Gamma_{g}}\left[\left(\mathbb{C}\nabla^{\mathrm{S}}\mathbf{u}\right)\cdot\mathbf{n}\right]\cdot\mathbf{w}d\Gamma \tag{25}$$

for every weighting function $\mathbf{w}\in[H^{1}(\Omega)]^{d_{s}}$, and integration by parts leads to eq. (23). Therefore, if the solution is sufficiently smooth, the test function $\mathbf{w}$ does *not* need to satisfy homogeneous Dirichlet boundary conditions in order for eq. (23) to be applicable.

Using the isoparametric approach, we seek an approximation $\mathbf{u}^{h}$ to the unknown exact solution field $\mathbf{u}$ of the elastostatic problem in the form

$$\mathbf{u}^{h}=\sum_{a=1}^{n}R_{a}\left(\mathbf{x}\right)\hat{\mathbf{u}}_{a} \tag{26}$$

where R_a are the NURBS basis functions described in Section 2.1 and representing the geometry of the problem, while $\hat{\mathbf{u}}_a$ are the unknown displacement control variables. Substitution into eq. (23) yields

$$\int_{\Omega}\left[\nabla\cdot\left(\mathbb{C}\nabla^{S}\mathbf{u}^{h}\right)+\mathbf{f}\right]\cdot\mathbf{w}d\Omega-\int_{\Gamma_{p}}\left[\left(\mathbb{C}\nabla^{S}\mathbf{u}^{h}\right)\cdot\mathbf{n}-\mathbf{p}\right]\cdot\mathbf{w}d\Gamma=0 \tag{27}$$

We now need a suitable choice for the test function $\mathbf{w}$, which, in a collocation method, is selected as the Dirac delta, that can be formally constructed as the limit of a sequence of smooth functions with compact support converging to a distribution (Auricchio et al., 2010a, 2012a) and satisfying the so-called sifting property, i.e.,

$$\int_{\Omega}f_{\Omega}\left(\mathbf{x}\right)\delta\left(\mathbf{x}-\mathbf{x}_{i}\right)d\Omega=f_{\Omega}\left(\mathbf{x}_{i}\right) \tag{28}$$

$$\int_{\Gamma}f_{\Gamma}\left(\mathbf{x}\right)\delta\left(\mathbf{x}-\mathbf{x}_{i}\right)d\Gamma=f_{\Gamma}\left(\mathbf{x}_{i}\right) \tag{29}$$

for every function f_Ω continuous about the point $\mathbf{x}_i\in\Omega$ and for every function f_Γ continuous about the point $\mathbf{x}_i\in\Gamma$. In the following, the Dirac delta will be indicated as a Dirac delta "function" following conventional terminology.

Let us assume that $d_s=2$, m_1 and m_2 are the numbers of control points in the two parametric directions, and $n=m_1m_2$ is the total number of control points. Thus $2n$ scalar equations are needed to determine the unknown displacement control variables. Analogously to the previous section, we choose n collocation points τ_{kl}, $k=\{1,...,m_1\}$, $l=\{1,...,m_2\}$ located

at the images of the (tensor product) Greville abscissae of the knot vectors. The collocation points for $k = 1, m_1$ and $l = 1, m_2$ are located at the boundary Γ. Separate sets of equations are needed for the patch interior and for the boundaries.

In the patch interior Ω, we write $2\,(m_1 - 2)\,(m_2 - 2)$ scalar equations by choosing as test functions the Dirac delta functions centered at the interior collocation points τ_{kl}, $k = \{2, ..., m_1 - 1\}$, $l = \{2, ..., m_2 - 1\}$. The resulting equations read

$$\left[\nabla \cdot \left(\mathbb{C}\nabla^S \mathbf{u}^h\right) + \mathbf{f}\right](\tau_{kl}) = \mathbf{0} \qquad \tau_{kl} \subset \Omega \tag{30}$$

i.e., they are the collocated strong form of the equations at τ_{kl}.

No equations are needed at the Dirichlet boundary, as we impose *a priori* that $u_i^h(\tau_{kl}) = g_i(\tau_{kl})$ on Γ_g.

To enforce Neumann boundary conditions, each $\tau_{kl} \subset \Gamma_p$ is associated with a collocation equation that sets the value of the boundary traction. This corresponds to choosing as test functions the Dirac delta functions centered at the collocation points located at the Neumann boundary. Here a distinction is needed between the collocation points located at the edges ($k = 1, m_1$ and $l = 2, ..., m_2 - 1$, or $l = 1, m_2$ and $k = 2, ..., m_1 - 1$), and those located at the corners of the domain ($k = 1, m_1$ and $l = 1, m_2$). For collocation points located on edges within the Neumann boundary, the equations are

$$\left[\left(\mathbb{C}\nabla^S \mathbf{u}^h\right) \cdot \mathbf{n} - \mathbf{p}\right](\tau_{kl}) = \mathbf{0} \qquad \tau_{kl} \subset \text{edge} \subset \Gamma_p \tag{31}$$

i.e., they are the collocated strong form of the Neumann boundary conditions at τ_{kl}. For collocation points located at corners where two Neumann boundaries meet, it has been shown in Auricchio et al. (2012a)[3] that the appropriate equations are

$$\left[\left(\mathbb{C}\nabla^S \mathbf{u}^h\right) \cdot \mathbf{n}' - \mathbf{p}'\right](\tau_{kl}) + \left[\left(\mathbb{C}\nabla^S \mathbf{u}^h\right) \cdot \mathbf{n}'' - \mathbf{p}''\right](\tau_{kl}) = \mathbf{0} \quad \tau_{kl} \equiv \text{corner} \subset \Gamma_p \tag{32}$$

where $\mathbf{n}'$ and $\mathbf{n}''$ are the unit outward normals of the edges meeting at the corner, and $\mathbf{p}'$ and $\mathbf{p}''$ are the respective imposed tractions.

It is important to remark that, in a recent paper by De Lorenzis et al. (2014b), it has been shown that the above approach to impose Neumann boundary conditions may lead to spurious oscillations in cases implying solutions of reduced regularity, when non-uniform meshes are adopted. There-

[3] In addition, interested readers may find in Auricchio et al. (2012a) a detailed discussion on the conditions to be imposed in more complicate situations like at the interfaces of multi-patch geometries.

fore alternative methods are needed, and in the same paper two possible (simple) alternative strategies to cure this issue are presented.

3.3 Numerical results.

We now present some numerical experiments showing the behavior of the proposed collocation formulation. In particular, we propose: i) a plane strain test, to show the fact that the convergence rates observed in 1D are attained also on mapped geometries in higher dimensions; ii) a two-material two-patch plane strain traction test, to show the fact that constant strain states are represented exactly (also in the case of multi-patch analysis); and iii) a 3D test on an elastic block, on which a performance comparison among IGA collocation and Galerkin IGA and FEA is carried out.

Plane strain clamped quarter of an annulus. As a first test, we consider a plane strain quarter of an annulus, as sketched in Figure 7, with internal and external radii equal to $R_1 = 1$ and $R_2 = 4$, respectively. The domain can be exactly represented by a single quadratic NURBS patch.

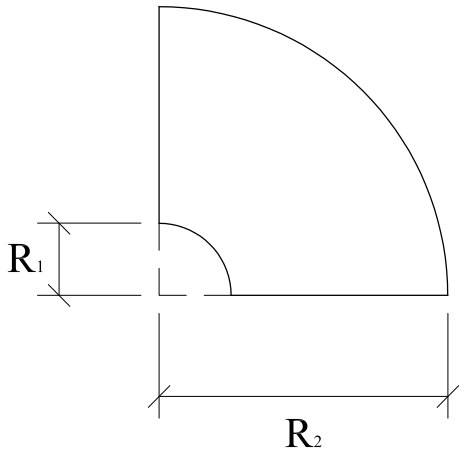

Figure 7. Plane strain clamped quarter of an annulus. Problem geometry.

The whole domain boundary is assumed to be clamped and we assign a

manufactured solution in terms of displacement components, reading:

$$\begin{cases} u = (x^2 + y^2 - 1)(x^2 + y^2 - 16)\sin(x)\sin(y), \\ v = (x^2 + y^2 - 1)(x^2 + y^2 - 16)\sin(x)\sin(y). \end{cases} \tag{33}$$

The manufactured solution satisfies the prescribed boundary conditions and the load is computed from it by imposing equilibrium.

The problem is solved by IGA collocation using Greville abscissae and in Figure 8 we present the results in terms of relative solution error in the L^2-norm versus the square root of the total number of control points. It is possible to observe that the convergence rates observed in the 1D case (i.e., p and $p-1$ for even and odd degree p, respectively) are attained.

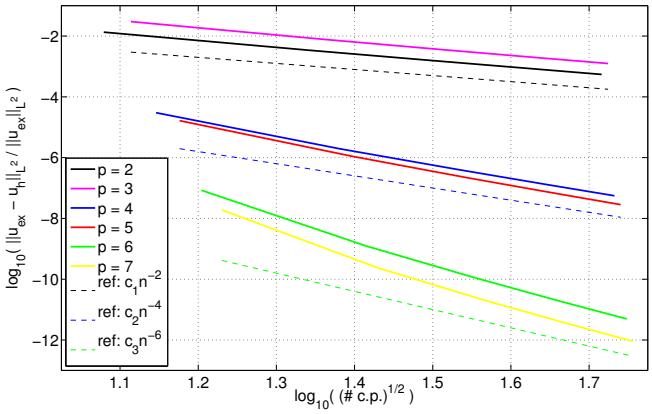

Figure 8. Plane strain clamped quarter of an annulus. Error plot versus the square root of number of control points for different degree NURBS.

Two-material two-patch plane strain traction test. We now consider a rectangular domain Ω, as sketched in Figure 9, subjected to a uniform traction. The domain is assumed to consist of two material subdomains.

The idea is to reproduce a solution homogeneous in the y direction (and piece-wise homogeneous in the x direction), such that the numerical results should be able to exactly reproduce the analytical solution. To obtain such a solution, it is necessary to properly calibrate the elastic constants. Accordingly, considering the standard plane strain equations for each material,

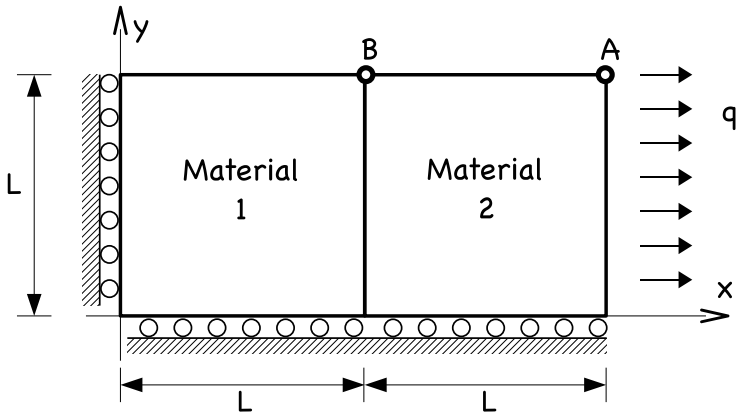

Figure 9. Two-material two-patch plane strain traction test. Problem geometry and boundary conditions.

we require the transverse strain (i.e., the strain in the transverse direction with respect to the traction direction) to be the same in both materials, obtaining the following relation

$$\frac{E_1}{E_2} = \frac{\nu_1 \left(1 + \nu_1\right)}{\nu_2 \left(1 + \nu_2\right)}$$

where the subscripts indicate the material numbers.

The problem under investigation is of particular interest also because it presents several noteworthy boundary conditions situations (e.g., it introduces a boundary point – point B in Figure 9 – with a combination of a traction-free boundary condition and an interface between different materials).

As material properties we assume $\nu_1 = 0.2$, $\nu_2 = 0.25$, and $E_2 = 1000$, resulting in $E_1 = 768$. With these choices, the exact displacement of point A (indicated in Figure 9) can be easily computed to be

$$u_A = 2.1875 \cdot 10^{-3} \quad v_A = 3.125 \cdot 10^{-4}$$

We numerically solve the problem by IGA collocation using two conforming NURBS patches (i.e., a patch for each material). The analytical solution is matched up to machine precision by the numerical one computed using a single element per patch, illustrating the good behavior of the proposed numerical scheme for the case under investigation.

Figure 10 shows the horizontal and vertical displacement fields (obtained using $p = q = 2$ and 3×3 control points per patch, i.e., one element per patch), which are linear in the two coordinate variables within each material, as expected. We also highlight that, as desired, a perfectly homogeneous solution is obtained in the y direction.

We may also notice that the management of a conforming multi-patch situation is very simple in the proposed collocation method, since it is based on constructing the discrete equilibrium relation for each patch and, then, summing the equations associated to collocation points shared by multiple patches (see Auricchio et al., 2012a, for more details).

3D elasticity test and comparison with Galerkin. We finally present the results of a 3D test on an elastic block, focusing in particular our attention on performance comparison among IGA collocation and Galerkin IGA and FEA. These results have been originally proposed by Schillinger et al. (2013), where a comprehensive study on the computational costs of IGA collocation as well as of Galerkin IGA and FEA is reported, including detailed operation counts showing the potential advantages of IGA collocation. Readers are therefore referred to such a paper for more details.

The considered problem consists of an elastic cube defined over the domain $[0, 1]^3$, fully clamped on its boundary and loaded by a body force giving rise to a manufactured solution $u_1 = u_2 = u_3 = \sin(2\pi x_1) \sin(2\pi x_2) \sin(2\pi x_3)$. Material parameters are selected to be $E = 1$ and $\nu = 0.3$.

Numerical results in terms of L^2- and H^1-norm relative errors versus number of degrees of freedom per parametric direction are reported in Figures 11 and 12, respectively. It is possible to see that, for IGA collocation, the same convergence rates observed in 1D are attained. For Galerkin IGA and FEA, instead, optimal convergence rates are attained, as expected from the theory. In terms of convergence constants, the best results are always guaranteed by Galerkin IGA, whereas IGA collocation presents slightly worse or similar results with respect to Galerkin FEA in the L^2-norm, and better results in the H^1-seminorm (except for the cubic case that, interestingly enough, in collocation is always underachieving, in particular with respect to the quadratic case).

Having in mind accuracy-to-computational-cost ratio as a measure of the efficiency of a numerical method, we also report results in terms of L^2- and H^1-norm relative errors versus computational times. The obtained results, reported in Figures 13 and 14, show that for degrees $p > 3$ IGA collocation guarantees the best overall performance, heavily outperforming Galerkin approaches in the H^1-seminorm. Such results are also supported by the operation counts provided in Schillinger et al. (2013). In particular,

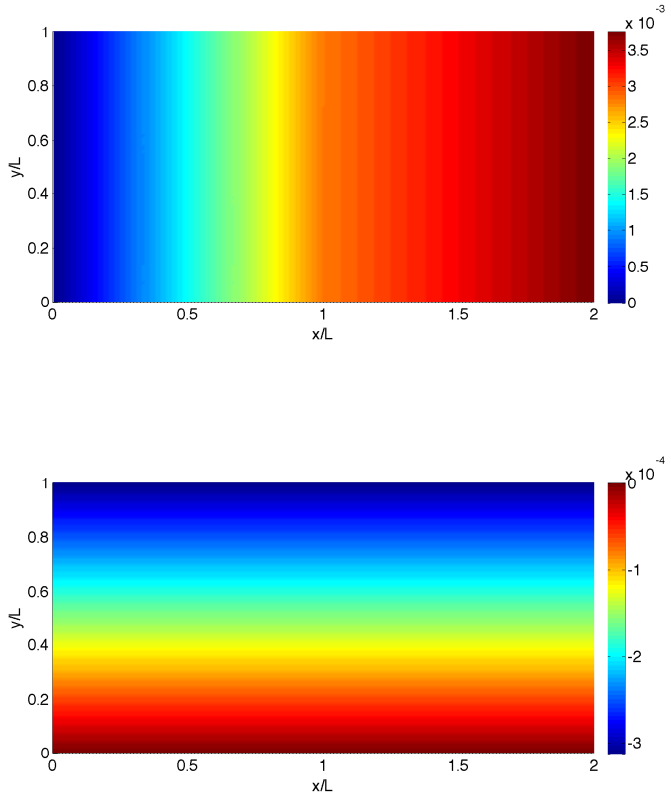

Figure 10. Two-material two-patch plane strain traction test. Horizontal (top) and vertical (bottom) displacement fields.

it is worth to remark that, as highlighted in the above-mentioned paper, the superiority of IGA collocation is best illustrated in Figure 14, where with $p = 4$ IGA collocation achieves an error level of 10^{-5} in the H^1-seminorm in less than 20 seconds, whereas both Galerkin approaches require more than 500 seconds to reach that accuracy.

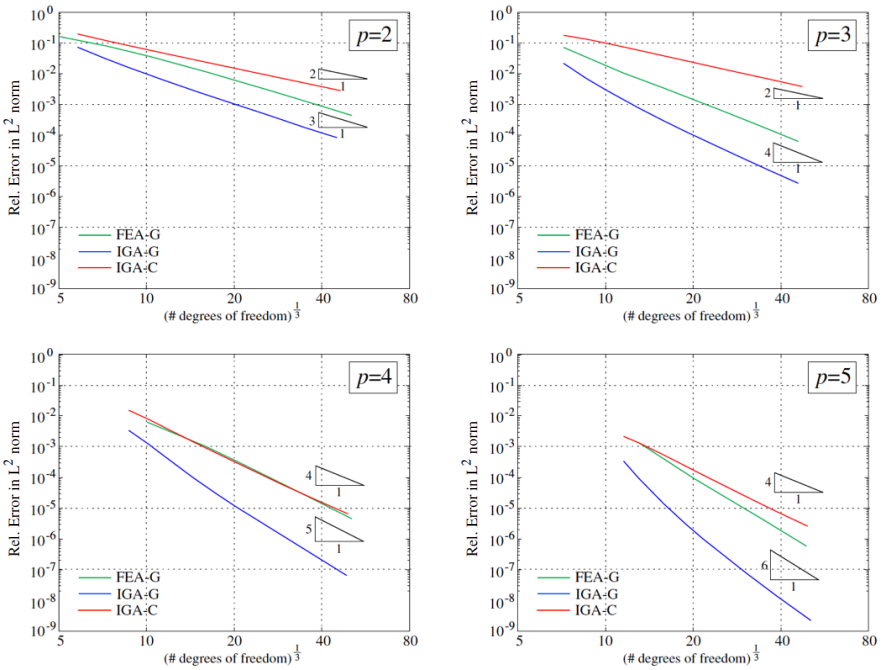

Figure 11. 3D elasticity test. Relative error in L^2-norm versus number of degrees of freedom per parametric direction for IGA collocation (IGA-C) as well as Galerkin IGA (IGA-G) and FEA (FEA-G).

4 A Brief Overview on Other Results and Applications

In this section, we give a brief overview on further results and interesting applications in the field of IGA collocation. Since the aim of the present chapter is just to give a basic and concise introduction to IGA collocation,

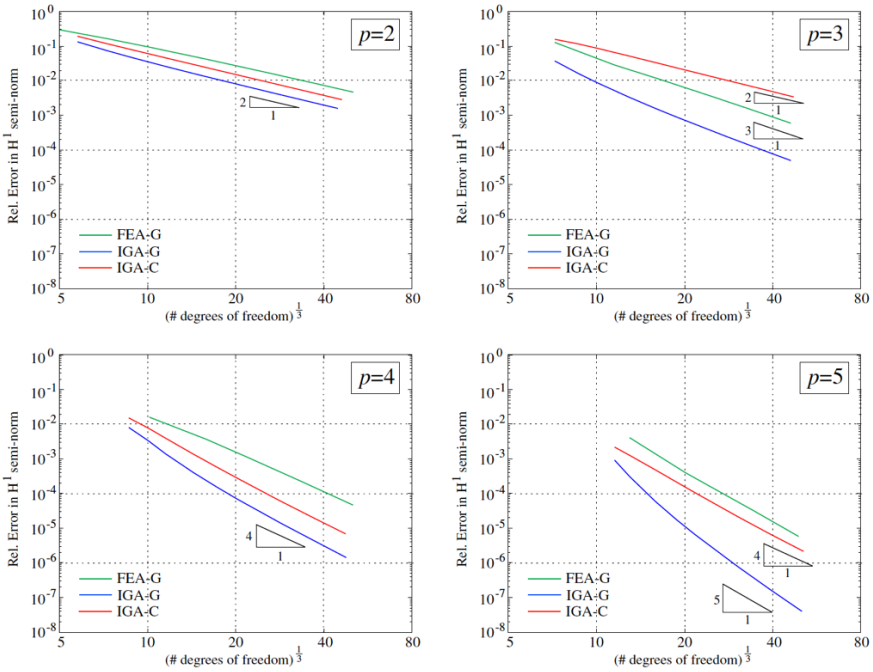

Figure 12. 3D elasticity test. Relative error in H^2-seminorm versus number of degrees of freedom per parametric direction for IGA collocation (IGA-C) as well as Galerkin IGA (IGA-G) and FEA (FEA-G).

this section is not meant as a complete and self-consistent review, and readers are referred to the cited individual papers for more information and details.

Explicit dynamics. Probably, the most promising application of IGA collocation is explicit dynamics. In fact, in explicit dynamics analyses, the speed is almost entirely dependent on the cost of quadrature, because the computational cost is dominated by stress divergence evaluations at quadrature points for the calculation of the residual force vector. Accordingly, explicit codes used extensively for crash dynamics and metal forming, such as LS-DYNA, rely almost exclusively on fast low-order quadrilateral and hexahedral elements with one-point quadrature. Unfortunately, those elements

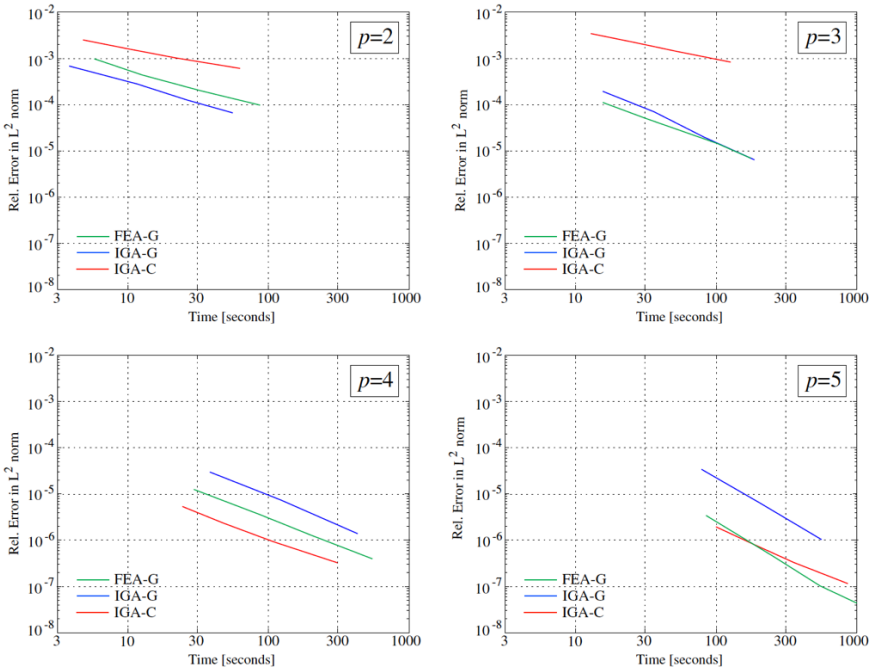

Figure 13. 3D elasticity test. Relative error in L^2-norm versus computational time for IGA collocation (IGA-C) as well as Galerkin IGA (IGA-G) and FEA (FEA-G).

typically require stabilization (whose parameters usually need fine-tuning by computationally expensive and time-consuming sensitivity studies) against mesh instabilities such as hourglass modes.

In this context, isogeometric collocation can be viewed as a one-point quadrature scheme that is rank sufficient and is therefore free of mesh instabilities. Hence, IGA collocation methods eliminate the need for ad hoc hourglass stabilization techniques and the relative parameter tunings, and can be seen as a very promising fast and accurate higher-order alternative (further considerations on the advantages of IGA collocation in explicit dynamics can be found in Auricchio et al., 2012a, and Schillinger et al., 2013). In addition, IGA collocation methods show great promise for the development of higher-order accurate time integration schemes due to the

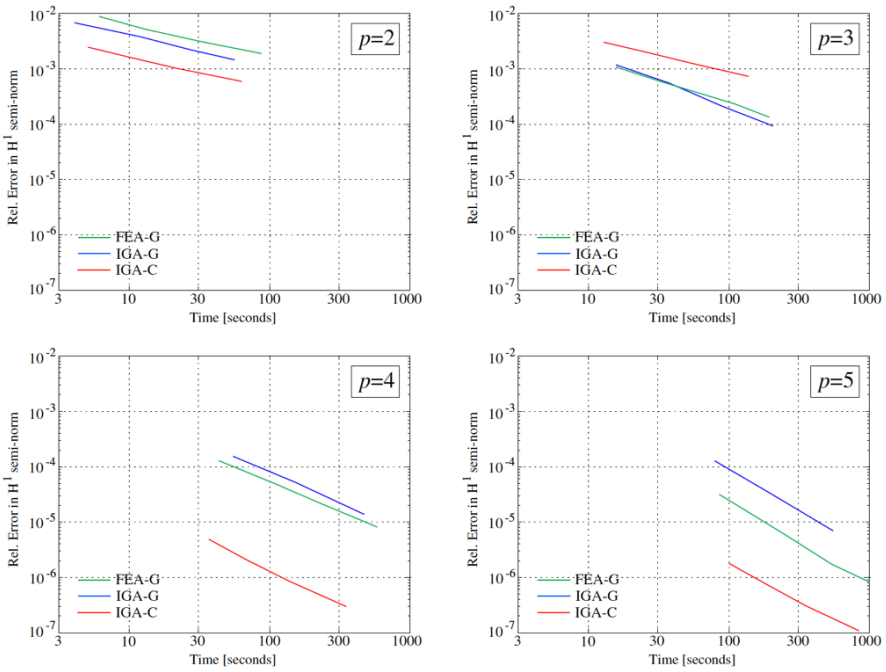

Figure 14. 3D elasticity test. Relative error in H^2-seminorm versus computational time for IGA collocation (IGA-C) as well as Galerkin IGA (IGA-G) and FEA (FEA-G).

convergence of the high modes in the eigenspectrum (cf. the spectral results in Section 2.2).

However, as in IGA Galerkin, classical row-sum mass lumping techniques limit accuracy of standard explicit schemes to second order only, independently of the approximation degree (Cottrell et al., 2006). In Auricchio et al. (2012a), a predictor-multicorrector scheme has been proposed to conveniently recover higher-order convergence rates in space within an explicit framework. Such a method is however only second-order in time. Moving from four-stage Runge-Kutta integration methods, similar results have been obtained also within a fourth order scheme in time (and preliminary results have been recently presented in Reali et al., 2014).

Local refinement. As we have seen, standard NURBS-based IGA collocation is based on tensor-product NURBS, which are used within the isoparametric paradigm for the representation of both geometry and field variables. Once the (tensor-product) geometry representation is fixed, also the distribution of the collocation points (e.g., Greville abscissae) is fixed and affected by the tensor-product structure. Therefore, when local refinement is needed, it is necessary to resort to alternative locally-refinable shape functions.

In Schillinger et al. (2013), this has been achieved resorting to hierarchical B-Splines and NURBS. However, in that paper, it has been shown that the plain use of those shape functions is not enough to get a working locally-refinable method, because linear independence problems may arise in transition regions between different levels. The proposed solution is to use hierarchical NURBS spaces in combination with the concept of weighted IGA collocation (practically applying the weighting concept only in transition regions). The resulting method is simple and efficient, and an accurate description can be found in Schillinger et al. (2013) along with several numerical tests proving its effectiveness. Among them, one of the most significant ones is a 3D advection-diffusion benchmark consisting of a cylinder that rotates around its axis with a tangential velocity $a_\theta = \omega r$ and a radial velocity $a_r = 0$, with a flow of constant axial velocity a_z, which results in a helical plume of the concentration that emerges from the fixed local inflow boundary condition $u = 1$. In Figure 15, we report the problem definition, the adopted hierarchical mesh (defined by an automatic adaptive refinement procedure based on a gradient-based error indicator), and the corresponding solution. A uniform discretization that yields a plume resolution with the same small element size as in the adaptive mesh requires a globally refined mesh with 1,095,200 degrees of freedom, whereas the presented adaptive mesh requires only 104,017 degrees of freedom.

Contact. When dealing with the simulation of practical structural mechanics problems involving interactions between multiple patches with nonconforming discretizations, the enforcement of contact constraints is a fundamental issue to be properly addressed. IGA contact is now an established research field in the Galerkin context, where it has been shown that the higher continuity typical of IGA shape functions can have beneficial effects (see, e.g., the recent review by De Lorenzis et al., 2014c, and references therein). More recently, the problem of frictionless contact has been successfully tackled also in the framework of IGA collocation by De Lorenzis et al. (2014b), who have proposed a two-half-pass algorithm. In that paper, several demanding examples have been considered in order to prove the

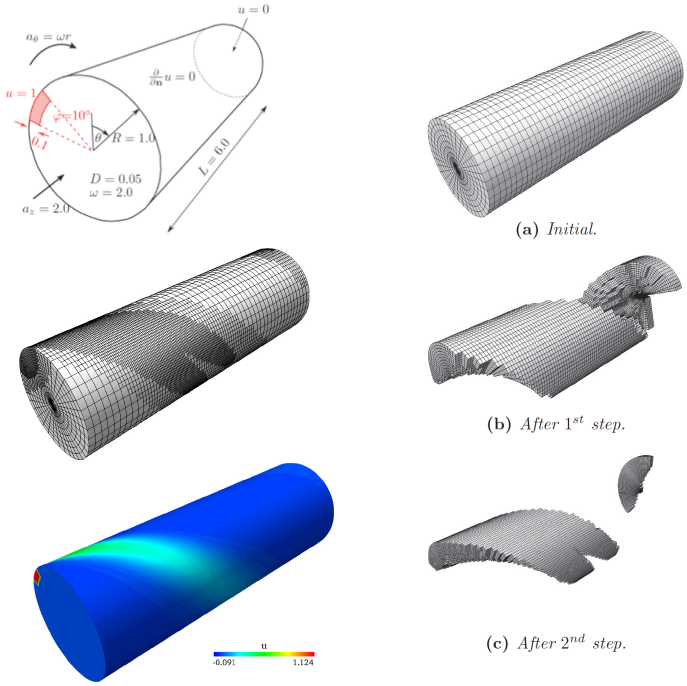

(a) *Initial.*

(b) *After* 1^{st} *step.*

(c) *After* 2^{nd} *step.*

Figure 15. Advection-diffusion in a rotating cylinder with hierarchical weighted collocation. Problem definition (top left); adopted hierarchical mesh (middle left); solution (bottom left); and finest elements at the different steps of the adaptive procedure (right).

good behavior of IGA collocation in contact problems. In particular, we mention here the remarkable fact that the contact patch test is passed up to machine precision with IGA collocation, something that does not happen for standard node-to-surface algorithms with Galerkin formulations.

Structural elements. The peculiar features of IGA collocation has been also widely applied for the development of structural thin elements like beams and plates. In particular, Bernoulli-Euler beam and Kirchhoff plate elements have been proposed by Reali and Gomez (2014). Also shear-deformable structural elements have been considered and, in the case of three-field (i.e., displacements, rotations, shear stresses) mixed formula-

tions for Timoshenko initially-straight planar beams (Beirão da Veiga et al., 2012) and for curved spatial rods (Auricchio et al., 2013), the structure of IGA collocation leads to mixed methods which are locking-free independently of the approximation degrees for the three fields. Such a unique property has been proven analytically and extensively tested numerically. Following those positive results, isogeometric collocation has been then successfully applied also to the solution of Reissner-Mindlin plate problems, in both primal and mixed forms Kiendl et al. (2014a). Finally, an interesting new single-parameter formulation for shear-deformable beams, recently introduced by Kiendl et al. (2014b), has been solved also via IGA collocation, and preliminary results on its plate counterpart have been shown in Kiendl et al. (2014c).

Phase-field modeling. IGA collocation has been finally employed as a fast, accurate, efficient, and geometrically flexible tool for phase-field models by Gomez et al. (2014). In particular, the considered model problem has been the Cahn-Hilliard equation, which is a central model in nonlinear interface dynamics and pattern formation, derived about fifty years ago as a model for phase separation of immiscible fluids by Cahn and Hilliard. Since then, it has been applied to a variety of physical problems, including planet formation, microstructure evolution of binary mixtures, and phase separation of polymer blend. The Cahn-Hilliard equation is also one of the simplest equations that can model stable co-existence of two phases and, as such, is the basis for various multiphase flow theories (interested readers are referred to the related references cited in Gomez et al., 2008, 2014). In the context of the numerical solution of the Cahn-Hiliard equation, IGA collocation proposes itself as a successful combination of the geometrical flexibility of Galerkin FEA and IGA approaches and the accuracy, efficiency, and simplicity of pseudo-spectral collocation methods. Several significant numerical examples are reported in Gomez et al. (2014), and two of them are shown in Figure 16. Given these positive results and the proven potential of phase-field modeling within the IGA framework (see, e.g., Gomez et al., 2008; Borden et al., 2012), this appears to be one of the most promising fields for the implementation of IGA collocation, in particular for what concerns the context of fracture mechanics (cf. De Lorenzis et al., 2014a, and Schillinger et al., 2014b).

5 Conclusions and further current developments.

The aim of this chapter was to give a concise introduction to the recently introduced and more than promising family of isogeometric methods based

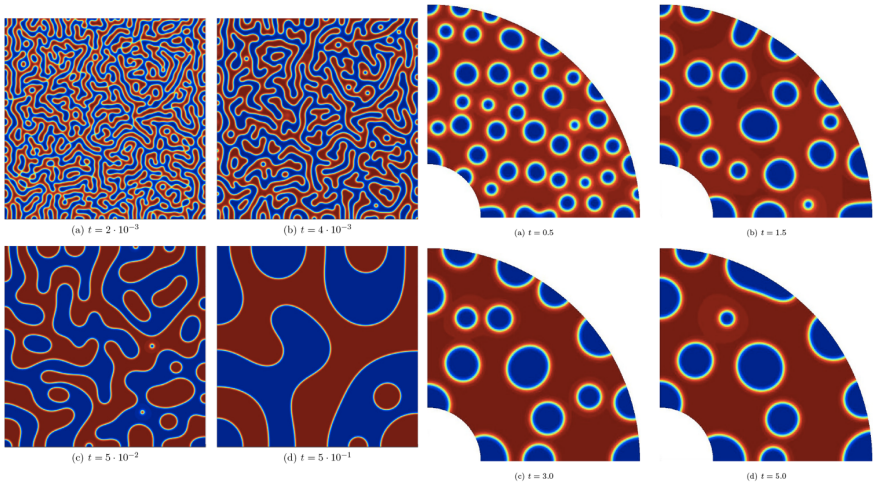

Figure 16. Phase-field modeling via IGA collocation. Spinodal decomposition on a square domain (left) and nucleation on a mapped domain (right). See Gomez et al. (2014) for details and parameter values.

on the collocation concept. Accordingly, the basic ideas of the approach have been first introduced in 1D along with some theoretical results, and then extended to higher dimensions in the framework of linear elastostatics problems. Moreover, several significant numerical tests have been shown, in order to confirm the good behavior and potential of the method, also on the basis of the accuracy-to-computational-cost ratio and in comparison with Galerkin approaches.

We have finally given a brief overview of further results and interesting applications of IGA collocation, including local refinement, contact, structural elements, and phase-field modeling. In addition to the above-mentioned applications, some promising preliminary results have been also recently obtained in dealing with the incompressibility constraint via mixed methods (Morganti et al., 2014), in the nonlinear elastic and inelastic regimes (De Lorenzis et al., 2014a), as well as in the field of Computational Fluid Dynamics (Evans et al., 2013).

As it can be seen, due to its special features, IGA collocation has shown so far a lot of potential in many fields of Computational Mechanics and

is attracting more and more attention among researchers. However, there are many issues that still have to be addressed and fully understood (e.g., a complete and sound mathematical analysis of the method is yet to be developed), and the door is definitely open for many further improvements and applications.

Bibliography

I. Akkerman, Y. Bazilevs, V. M. Calo, T. J. R. Hughes, S. Hulshoff. The role of continuity in residual-based variational multiscale modeling of turbulence. *Computational Mechanics*, 41:371–378, 2007.

F. Auricchio, L. Beirão da Veiga, A. Buffa, C. Lovadina, A. Reali, and G. Sangalli. A fully "locking-free" isogeometric approach for plane linear elasticity problems: A stream function formulation. *Computer Methods in Applied Mechanics and Engineering*, 197:160–172, 2007.

F. Auricchio, L. Beirão da Veiga, T.J.R. Hughes, A. Reali, and G. Sangalli. Isogeometric collocation methods. *Mathematical Models and Methods in Applied Sciences*, 20(11):2075–2107, 2010.

F. Auricchio, L. Beirão da Veiga, T.J.R. Hughes, A. Reali, and G. Sangalli. Isogeometric collocation for elastostatics and explicit dynamics. *Computer Methods in Applied Mechanics and Engineering*, 249-252:2–14, 2012.

F. Auricchio, L. Beirão da Veiga, J. Kiendl, C. Lovadina, and A. Reali. Locking-free isogeometric collocation methods for spatial Timoshenko rods. *Computer Methods in Applied Mechanics and Engineering*, 263:113–126, 2013.

F. Auricchio, L. Beirão da Veiga, C. Lovadina, A. Reali. The importance of the exact satisfaction of the incompressibility constraint in nonlinear elasticity: mixed FEMs versus NURBS-based approximations. *Computer Methods in Applied Mechanics and Engineering*,199:314–323, 2010.

F. Auricchio, F. Calabrò, T.J.R. Hughes, A. Reali, and G. Sangalli. A simple algorithm for obtaining nearly optimal quadrature rules for NURBS-based isogeometric analysis. *Computer Methods in Applied Mechanics and Engineering*, 249–252:15–27, 2012.

Y. Bazilevs, V.M. Calo, J.A. Cottrell, T.J.R. Hughes, A. Reali, G. Scovazzi. Variational multiscale residual-based turbulence modeling for large eddy simulation of incompressible flows. *Computer Methods in Applied Mechanics and Engineering*, 197:173–201, 2007.

Y. Bazilevs, T.J.R. Hughes. NURBS-based isogeometric analysis for the computation of flows about rotating components. *Computational Mechanics*, 43:143–150, 2008.

L. Beirão da Veiga, T.J.R. Hughes, J. Kiendl, C. Lovadina, J. Niiranen, A. Reali, and H. Speelers. A locking-free model for Reissner-Mindlin plates: Analysis and isogeometric implementation via NURBS and triangular NURPS. *In preparation*, 2014.

L. Beirão da Veiga, C. Lovadina, and A. Reali. Avoiding shear locking for the Timoshenko beam problem via isogeometric collocation methods. *Computer Methods in Applied Mechanics and Engineering*, 241-244:38–51, 2012.

M.J. Borden, C.V. Verhoosel, M.A. Scott, T.J.R. Hughes, C.M. Landis. A phase-field description of dynamic brittle fracture. *Computer Methods in Applied Mechanics and Engineering*, 217:77–95, 2012.

J.F. Caseiro, R.A.F. Valente, A. Reali, J. Kiendl, F. Auricchio, R.J. Alves de Sousa. On the Assumed Natural Strain method to alleviate locking in solid-shell NURBS-based finite elements. *Computational Mechanics*, 53:1341–1353, 2014.

J.A. Cottrell, T.J.R. Hughes, Y. Bazilevs. *Isogeometric Analysis: Toward Integration of CAD and FEA*. Wiley, 2009.

J.A. Cottrell, T.J.R. Hughes, A. Reali. Studies of refinement and continuity in isogeometric structural analysis. *Computer Methods in Applied Mechanics and Engineering*,196:4160–4183, 2007.

J.A. Cottrell, A. Reali, Y. Bazilevs, and T.J.R. Hughes. Isogeometric analysis of structural vibrations. *Computer Methods in Applied Mechanics and Engineering*, 195:5257–5296, 2006.

A. Buffa, C. de Falco, G. Sangalli. IsoGeometric Analysis: Stable elements for the 2D Stokes equation. *International Journal for Numerical Methods in Fluids*, 65:1407–1422, 2011.

C. de Boor. *A practical guide to Splines (revised edition)*. Springer, 2001.

C. de Falco, A. Reali, R. Vázquez. GeoPDEs: a research tool for IsoGeometric Analysis of PDEs. *Advances in Engineering Software*, 42:1020–1034, 2011.

L. De Lorenzis, M. Ambati, J.A. Evans, T.J.R. Hughes, R. Kruse, N. Nguyen-Thanh, A. Reali. *Recent results on isogeometric collocation for the solution of non-linear problems*. Invited lecture at HOFEIM 2014 – Workshop on Higher Order Finite Element and Isogeometric Methods, Munich, July 15-18, 2014.

L. De Lorenzis, J.A. Evans, T.J.R. Hughes, A. Reali. Isogeometric collocation: Neumann boundary conditions and contact. *Computer Methods in Applied Mechanics and Engineering*, doi:10.1016/j.cma.2014.06.037, 2014.

L. De Lorenzis, T.J.R. Hughes, P. Wriggers. Isogeometric contact: a review. *GAMM MItteilungen*, 37:85–123, 2014.

S. Demko. On the existence of interpolation projectors onto spline spaces, *Journal of Approximation Theory*, 43:151–156, 1985.

R.P. Dhote, H. Gomez, R N.V. Melnik, J. Zu. Isogeometric analysis of a dynamic thermo-mechanical phase-field model applied to shape memory alloys. *Computational Mechanics*, 53:1235–1250, 2014.

T. Elguedj, Y. Bazilevs, V.M. Calo, T.J.R. Hughes. $\bar{B}$ and $\bar{F}$ projection methods for nearly incompressible linear and non-linear elasticity and plasticity using higher-order NURBS elements. *Computer Methods in Applied Mechanics and Engineering*, 197:2732–2762, 2008.

J.A. Evans, R. Hiemstra, T.J.R. Hughes, D. Schillinger. *Isogeometric Divergence-Conforming Collocation Methods for Incompressible Fluid Flow.* Invited lecture at the 12th U.S. National Congress on Computational Mechanics, Raleigh, July 22-25, 2013.

H. Gomez, V. M. Calo, Y. Bazilevs, and T. J. R. Hughes. Isogeometric analysis of the Cahn–Hilliard phase-field model. *Computer Methods in Applied Mechanics and Engineering*, 197:4333–4352, 2008.

H. Gomez, T.J.R. Hughes, X. Nogueira, V.M. Calo. Isogeometric analysis of the isothermal Navier-Stokes-Korteweg equations. *Computer Methods in Applied Mechanics and Engineering*, 199:1828–1840, 2010.

H. Gomez, A. Reali, and G. Sangalli. Accurate, efficient, and (iso)geometrically flexible collocation methods for phase-field models. *Journal for Computational Physics*, 262:153–171, 2014.

T.J.R. Hughes, J.A. Cottrell, and Y. Bazilevs. Isogeometric analysis: CAD, finite elements, NURBS, exact geometry, and mesh refinement. *Computer Methods in Applied Mechanics and Engineering*, 194:4135–4195, 2005.

T.J.R. Hughes, J.A. Evans, A. Reali. Finite Element and NURBS Approximations of Eigen- value, Boundary-value, and Initial-value Problems. *Computer Methods in Applied Mechanics and Engineering*, 272:290–320, 2014.

T.J.R. Hughes, A. Reali, and G. Sangalli. Duality and unified analysis of discrete approximations in structural dynamics and wave propagation: Comparison of p-method finite elements with k-method NURBS. *Computer Methods in Applied Mechanics and Engineering*, 197:4104–4124, 2008.

T.J.R. Hughes, A. Reali, and G. Sangalli. Efficient quadrature for NURBS-based isogeometric analysis. *Computer Methods in Applied Mechanics and Engineering*, 199:301–313, 2010.

J. Kiendl, F. Auricchio, L. Beirao da Veiga, C. Lovadina, A. Reali. Isogeometric collocation methods for the Reissner-Mindlin plate problem. Submitted, 2014.

J. Kiendl, F. Auricchio, T.J.R. Hughes, A. Reali. Single-variable formulations and isogeometric discretizations for shear deformable beams. ICES Report 14-26, 2014.

J. Kiendl, F. Auricchio, T.J.R. Hughes, A. Reali. *Isogeometric one-parameter formulations for shear deformable structures.* Keynote lecture at WCCM-ECCM-ECFD2014 – 11th World Congress on Computational Mechanics, 5th European Conference on Computational Methods, and 6th European Conference on Computational Fluid Dynamics, Barcelona, July 20-25, 2014.

J. Kiendl, K.-U. Bletzinger, J. Linhard, and R. Wüchner. Isogeometric shell analysis with Kirchhoff-Love elements. *Computer Methods in Applied Mechanics and Engineering*, 198:3902–3914, 2009.

S. Lipton, J.A. Evans, Y. Bazilevs, T. Elguedj, T.J.R. Hughes. Robustness of isogeometric structural discretizations under severe mesh distortion. *Computer Methods in Applied Mechanics and Engineering*, 199:357–373, 2010.

J. Liu, H. Gomez, J.A. Evans, T.J.R. Hughes, C.M. Landis. Functional entropy variables: A new methodology for deriving thermodynamically consistent algorithms for complex fluids, with particular reference to the isothermal Navier-Stokes-Korteweg equations. new block *Journal of Computational Physics*, 248:47–86, 2014.

S. Morganti, F. Auricchio, D.J. Benson, F.I. Gambarin, S. Hartmann, T.J.R. Hughes, A. Reali. Patient-specific isogeometric structural analysis of aortic valve closure. *ICES Report*, 14-10, 2014.

S. Morganti, F. Auricchio, L. De Lorenzis, J.A. Evans, T.J.R. Hughes, A. Reali. *Isogeo- metric collocation: incompressible elasticity, locking and possible solutions.* Invited lecture at WCCM-ECCM-ECFD2014 – 11th World Congress on Computational Mechanics, 5th European Conference on Computational Methods, and 6th European Conference on Computational Fluid Dynamics, Barcelona, July 20-25, 2014.

L. Piegl, W. Tiller. The NURBS Book, 2nd Edition. Springer-Verlag, 1997.

A. Reali. An isogeometric analysis approach for the study of structural vibrations. *Computer Methods in Applied Mechanics and Engineering*, 1–30:15–27, 2006.

A. Reali, H. Gomez. An isogeometric collocation approach for Bernoulli-Euler beams and Kirchhoff plates. *Submitted*, 2014.

A. Reali, J.A. Evans, T.J.R. Hughes. *Isogeometric Analysis: Structural vibrations and dynamics.* Semi-plenary lecture at WCCM-ECCM-ECFD2014 – 11th World Congress on Computational Mechanics, 5th European Conference on Computational Methods, and 6th European Conference on Computational Fluid Dynamics, Barcelona, July 20-25, 2014.

D. Schillinger, J.A. Evans, A. Reali, M.A. Scott, T.J.R. Hughes. Isogeometric collocation: Cost comparison with Galerkin methods and extension to adaptive hierarchical NURBS discretizations. *Computer Methods in Applied Mechanics and Engineering*, 267:170–232, 2013.

D. Schillinger, S.J. Hossain, T.J.R. Hughes. Reduced Bézier element quadrature rules for quadratic and cubic splines in isogeometric analysis. *Computer Methods in Applied Mechanics and Engineering*, 277:1–45, 2014.

D. Schillinger, J.A. Evans, T.J.R. Hughes. *Cost of collocation, accuracy of Galerkin: On the potential of higher-order collocation-type methods in IGA and hp FEM.* Invited lecture at HOFEIM 2014 – Workshop on Higher Order Finite Element and Isogeometric Methods, Munich, July 15-18, 2014.